January 17, 2013 (Web) DOI: 10.1021/la304602e

Langmuir

Article

pubs.acs.org/Langmuir

Dynamic Domains in Polymersomes: Mixtures of Polyanionic and Neutral Diblocks Respond More Rapidly to Changes in Calcium than to pH

Kyle Spinler,[†] Aiwei Tian,[†,‡] David A. Christian,[†] Diego A. Pantano,[†] Tobias Baumgart,*[,†,‡,§] and Dennis E. Discher*[,†,§]

[†]Department of Chemical and Biomolecular Engineering, [‡]Department of Chemistry, and [§]Laboratory for Research on the Structure of Matter, Materials Research Science and Engineering Center, University of Pennsylvania, Philadelphia, Pennsylvania 19104, United States

ABSTRACT: Chemical triggering of membrane domain dynamics is of broad relevance to cell signaling through lipid bilayers and might also be exploited in application of phase-separated vesicles. Here we describe the morphodynamics and remixing kinetics of spotted polymersomes made with mixtures of polyanionic and neutral amphiphiles plus calcium. Addition of the calcium chelator EDTA to vesicle dispersions produced a decrease in domain size within minutes, whereas increasing the pH with NaOH led to the viscous fingering of domains and decreased domain size over hours. Although the latter suggests that the charge of the polyanion contributes to domain formation, the remixing of more negative chains at high pH is surprising. Domain roughening at high pH is also accelerated by EDTA, which highlights the dominance of cross-bridging. Importantly, even though vesicles were perturbed only externally, the inner and outer leaflets remain coupled throughout, consistent with molecular dynamics simulations and suggestive of an order−disorder transition that underlies the remixing kinetics.

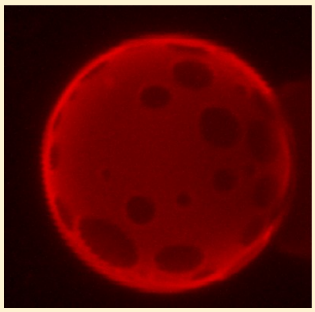

1. INTRODUCTION

Heterogeneity in membrane phases is of interest in various biological processes such as vesicle trafficking and signal transduction, but it is difficult to elucidate the role that phase separation plays in cell function because of the compositional complexity of biomembranes. However, a deep understanding of phase behavior within vesicles made of lipid or polymer amphiphiles is possible because of their simplicity. Bilayer liposomes or polymersomes can also encapsulate therapeutics for drug delivery applications,[1,2] so studies of vesicle phase behavior have the potential to advance biological insight as well as biomedical applications.

Giant unilamellar vesicles have been intensely studied as model membranes for years and exhibit well-characterized phase behavior.[3−5] Domain dynamics have been examined mostly under physical perturbations such as temperature,[5−7] osmotic pressure,[8] and curvature.[9] Although lipid membranes are fusogenic under electrolyte perturbations, mesoscale phase separation in lipid vesicles induced by hydrophilic immiscibility (e.g., electrostatic interactions) is still debated,[10,11] and hydrophobic immiscibility should be inert to ionic strength changes. Domain dynamics due to changes in high-valence salts and/or pH are thus understudied.

Polymersomes made with mixtures of amphiphillic diblock copolymers offer some advantages in studies of domains. These vesicles are very stable mechanically and thermodynamically compared to liposomes,[12−14] so studies of domain morphology upon chemical perturbation are feasible. Furthermore, the use of weak polyelectrolytes in block copolymers makes possible a susceptibility to changes in pH and ionic strength. Although kinetic investigations on the effects of pH and salt on assemblies of weak polyelectrolytes have been carried out with block copolymer brushes, micelles, and vesicles,[15−22] domain dynamics in polymersome membranes have remained unstudied.

We recently described spotted polymersomes in a quasi-equilibrium state composed of a binary mixture of neutral poly(ethylene oxide)−polybutadiene (OB18) and negatively charged poly(acrylic acid)−polybutadiene (AB1).[23] Divalent cations (e.g., calcium, copper, and barium) in solution electrostatically cross-bridge the anionic AB1 chains and induce the lateral segregation of the AB1 chains into domains. We observed the stability of these domains at room temperature for at least a year but had not previously studied their dynamics. Additionally, phase separation was also seen in only a surprisingly narrow range of solution pH and calcium concentration. This suggested the potential for rapid domain dynamics with changes in pH and calcium content.

Here we provide novel evidence of what is seen with spotted polymersomes when the solution pH and calcium are quickly shifted to regimes well outside those suited for lateral segregation. Domain mixing kinetics were obtained upon removal of calcium from the outer leaflet of AB1-rich domains by adding EDTA, a strong calcium-chelating reagent. Viscous fingering, domain bulging, and decreases in the AB1-rich domain

Special Issue: Interfacial Nanoarchitectonics

Received: November 18, 2012
Revised: January 15, 2013

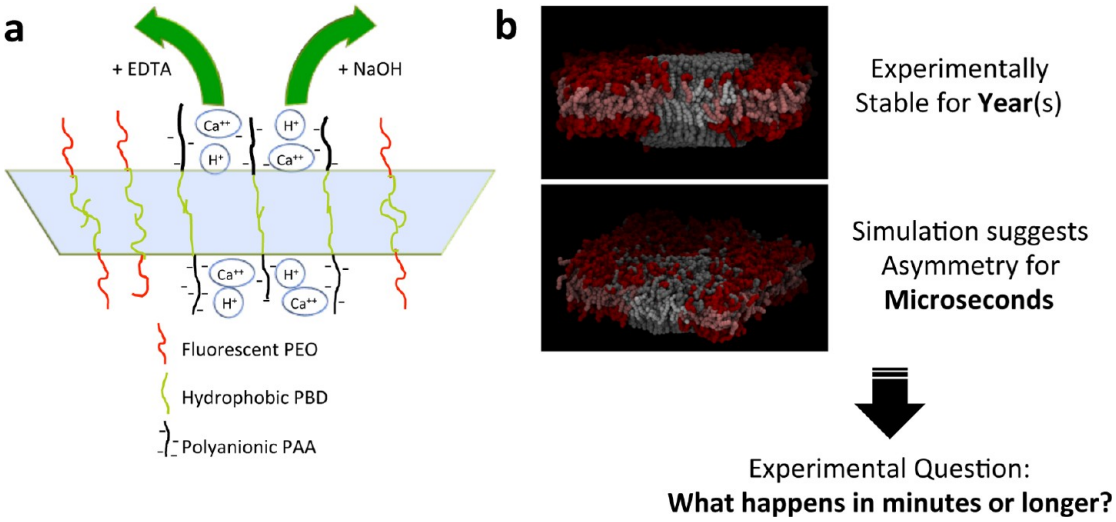

Figure 1. (a) Schematic illustration of EDTA and NaOH applications to the AB1-rich domain. EDTA and NaOH remove Ca^{2+} and H^+ from PAA chains, respectively. (b) Coarse-grained molecular dynamics simulation of inner and outer leaflet coupling in phase-separated bilayers facilitated by a molecular cross-linker. The upper image is such a bilayer in the presence of a cross-linker. The lower image is the result of the removal of cross-linker from the upper leaflet. Molecular interdiffusion is observed in the upper leaflet, and the lower leaflet remains phase-separated.

area fraction were seen after increasing the external pH by adding NaOH. We also saw that EDTA accelerated the domain boundary roughening processes induced by NaOH. Throughout, interleaflet registration was evident with these perturbations to the solutions outside these low-permeability vesicles, in agreement with modeling by coarse-grained molecular dynamics that revealed the underlying nature of chain-ordering transitions.[24] The separation of time scales between calcium cross-bridging and polyanion charge set by pH thus reflects the kinetics of this order−disorder transition.

2. EXPERIMENTAL SECTION

2.1. Materials. Block copolymers of poly(ethylene oxide)−poly(butadiene) (PEO_{80}−PBD_{125}) denoted as OB18 (M_w = 10 400 g/mol) and poly(acrylic acid)−poly(butadiene) (PAA_{75}−PBD_{103}) denoted as AB1 (M_w = 10 050 g/mol) were made as described.[23] OB18 was labeled with tetramethylrhodamine (TMR) and denoted as OB18*.

2.2. Preparation of Phase-Separated Polymersomes. Phase-separated polymersomes were formed via film hydration as described[23] at pH 3.5 with $[Ca^{2+}]$ = 0.1 mM at a total polymer concentration of 0.1 mg/mL.

2.3. Leaflet Asymmetric Treatment of Phase-Separated Polymersomes. After phase-separated vesicle formation, an ∼50 μL vesicle dispersion was transferred to an imaging chamber. A single phase-separated vesicle was immobilized by means of micropipet aspiration while being imaged with confocal microscopy over a time course of minutes to hours. Vesicle imaging and manipulation were performed as described.[25] EDTA or an EDTA/NaOH = 1.8 mol/mol aqueous solution was injected into the chamber through a 10 μL syringe (Hamilton, Reno, NV) while imaging. Because of the slow kinetics of domains subject to NaOH treatment, vesicles were allowed to incubate with NaOH in Eppendorf tubes for more than 4 h (typically overnight) and were then transferred to the imaging chamber.

2.4. Imaging. Phase-separated polymersomes were imaged by *xyz* scanning using a laser scanning confocal fluorescence microscope (Olympus, FV300) with a 60× water-immersion objective (Olympus). TMR was excited using a 543 nm laser.

2.5. Image Analysis. Hemisphere projections of vesicles were obtained by combining *z*-stack images using an Olympus Fluoview 300. Quantitative analysis of images was performed through MATLAB (Mathworks, Natick, MA) and ImageJ (National Institutes of Health, Bethesda, MD).

3. RESULTS

Polymer vesicles have thick, highly stable membranes that are significantly less permeable to ions when compared to lipid membranes.[14,26,27] Therefore, changes in the ion concentration and pH in the solution outside the polymer vesicle result in an asymmetric environment of the membrane as the aqueous lumen of the vesicle, which contacts the inner leaflet, remains unchanged. Here, we tested the effects of pH and calcium concentration changes on polymersome domains by monitoring the domain kinetics after the asymmetric addition of EDTA and/or NaOH solutions, which should undermine the cross-linking within the domains and thereby affect the stability (Figure 1). EDTA and NaOH remove Ca^{2+} and H^+, respectively, from the outer leaflet of AB1-rich domains of polymer vesicles, and these changes are shown to have dramatic effects on the domain morphology.

3.1. Removing Calcium Cross-Bridges from PAA Chains by EDTA Addition. Calcium cross-bridges weak polyanion chains (e.g., PAA) in polyelectrolyte gels,[28] brushes,[18] and the hydrophilic brushes of PAA−PBD (AB1) vesicles.[23] This cross-bridging between AB1 chains mediates the domain formation in polymersomes containing neutral PEO−PBD (OB18).[23] Therefore, removing calcium would lead to domain dissolution. To test the domain remixing kinetics after calcium removal from the outer leaflet of the membrane, excess EDTA (0.36−0.96 mM) was added to the vesicle dispersion (originally containing 0.1 mM Ca^{2+}). The resulting calcium concentrations were calculated from the equilibrium constant of the EDTA−calcium complex and pH-dependent fractional compositions of EDTA (fraction of free EDTA).[29] As predicted, domain remixing was observed within minutes after EDTA addition, and vesicles became homogeneous within minutes to hours.

Dark AB1-rich domains mix with OB18*-rich domains mainly though an area shrinking process. To quantify the domain mixing kinetics, vesicles with a 25 or 60% mixing weight ratio of AB1 were examined. Domain dynamics after EDTA addition are depicted in Figure 2, where AB1-rich domains display an area shrinking process as they begin to mix with OB18* domains (Figure 2a,b). Interestingly, fluorescence intensities at shrinking

dx.doi.org/10.1021/la304602e | *Langmuir* XXXX, XXX, XXX−XXX

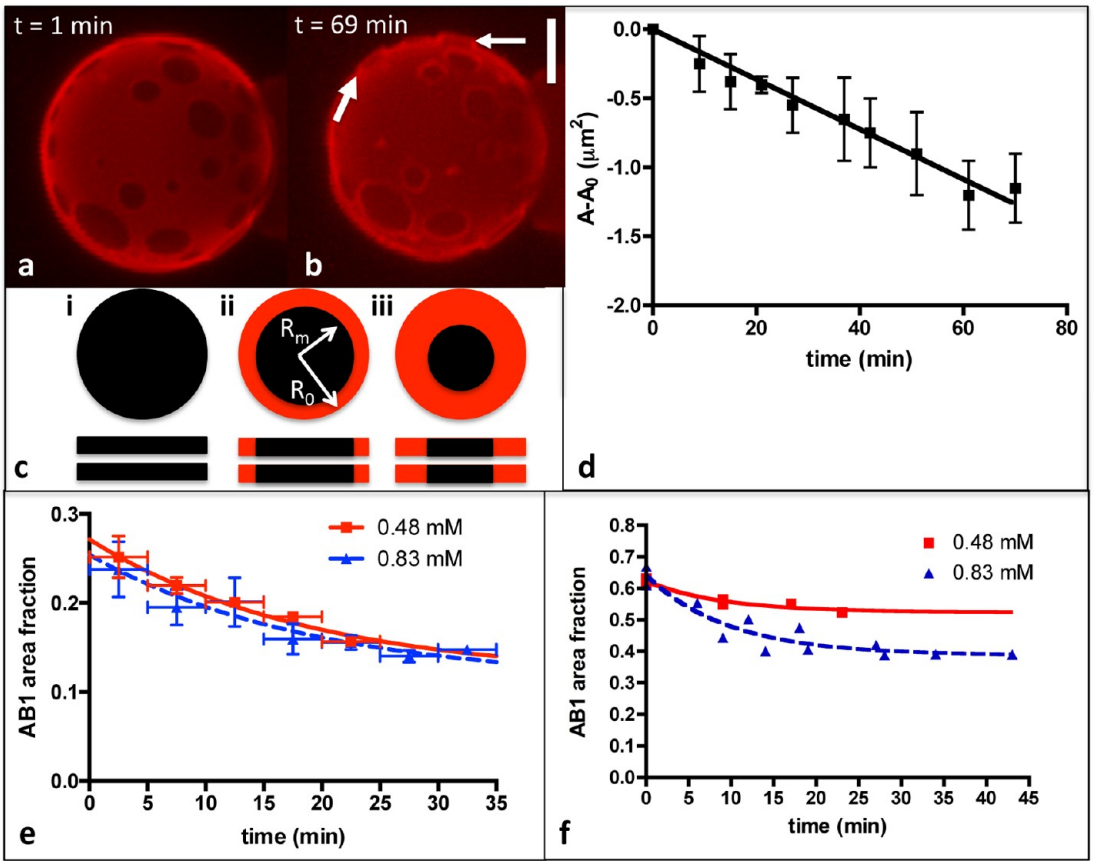

Figure 2. Domain mixing after EDTA addition. (a, b) Confocal z stacks displaying the top hemisphere of a phase-separated vesicle (AB1/OB18* = 25:75) with multiple domains (a) 1 and (b) 69 min after adding EDTA to the vesicle dispersion (reaching a final EDTA concentration of 0.83 mM). AB1-rich domain shrinking was observed. In addition, AB1-rich domains invaded by OB18* bend outward from the vesicle (indicated by arrows), which causes the artifact of a bright circle at the domain boundary. The scale bar is 5 μm. (c) Schematic drawings illustrating the process of the domain area shrinking mechanism. R_0 is the original AB1 domain radius at $t = 0$, and R_m is the radius of the melting AB1 boundary. Stage I shows the AB1 domain before EDTA treatment. Stages ii and iii demonstrate the process of the OB18*-rich domain invading the AB1-rich domain with time. (d) Plot of domain area change ($A - A_0$) vs time upon adding EDTA. The solid line is the fitting using eq 2, from which we calculated the interdiffusion coefficient of OB18* to be $D = (2.3 \pm 0.5) \times 10^{-5}$ μm^2/s (av ± S.D., $N_{domain} = 17$, $N_{vesicle} = 4$). (e) EDTA treatment of 25 wt % AB1 vesicles. Red squares and blue triangles are the results of 0.48 and 0.83 mM EDTA additions, respectively. Fit of time, t, for 0.48 mM: $y = 0.16 \exp[-t/19] + 0.12$, $R^2 = 0.87$, $N_{vesicle} = 3$. Fit of t for 0.83 mM: $y = 0.14 \exp[-t/19] + 0.11$, $R^2 = 0.75$, $N_{vesicle} = 4$. (f) EDTA treatment of 60 wt % AB1 vesicles. Red squares and blue triangles are the results of 0.48 and 0.83 mM EDTA additions, respectively. Fit of t for 0.48 mM: $y = 0.01 \exp[-t/8.9] + 0.52$, $R^2 = 0.94$, $N_{vesicle} = 3$. Fit of t for 0.83 mM: $y = 0.25 \exp[-t/9.8] + 0.39$, $R^2 = 0.88$, $N_{vesicle} = 4$.

domain boundaries appear to be greater than for the surrounding OB18*-rich domains because of the membrane curvature at domain boundaries (arrows in Figure 2b). When calcium is removed from the outer leaflet, PAA chains in the outer leaflet are expected to expand,[18] which leads to a larger AB1-rich domain area of the outer leaflet compared to that of the inner leaflet. This area difference would lead to outward AB1-rich domain budding. However, AB1-rich domain boundaries have mixed with OB18* and hence are softer than the center of AB1-rich domains. Therefore, we observed only boundary curvature effects instead of bulk domain bulging. Aside from the increased fluorescence intensity at the domain boundary, only two levels of fluorescence intensity were observed in the membrane: OB18*-rich domains (bright red) and AB1-rich domains (dim red). No intermediate level of fluorescence intensity was seen indicating complete registration between the outer and inner leaflets of the membrane. Therefore, we propose that interleaflet coupling is maintained during asymmetric leaflet chemical stimuli. Subsequent coarse-grained molecular dynamics simulation confirmed this hypothesis.[24]

The phenomenon of varying the outer leaflet chemical environment leading to the change in both leaflets is also observed by the Keller group while applying β-cylcodextrin to deplete cholesterol from the outer leaflet of giant lipid vesicles[5] as well as by Samsonov et. al., who found that the addition of cholesterol oxidase to one side of a supported bilayer affected the phase behavior in both monolayers.[30] The above domain-coupling examples could be due to cholesterol's ability to flip-flop within lipid bilayers. However, the asymmetric leaflet domain registration of lipid membranes has also been documented, ruling out cholesterol flip-flop.[31]

The inner and outer leaflet domain coupling (leaflet registration) and domain shrinking kinetics under EDTA addition are illustrated in the schematic drawings of Figure 2c. Because of the high molecular weight of diblock copolymers and the resulting chain entanglement in the vesicle bilayer,[32] the rate-limiting step of domain mixing can be considered to be polymer interdiffusion instead of the removal of calcium cross-bridges by excess EDTA. The shrinkage of the domain area is consistent with the interdiffusion process during the demixing−remixing transition of polymer blends upon annealing.[33] To obtain the

dx.doi.org/10.1021/la304602e | Langmuir XXXX, XXX, XXX−XXX

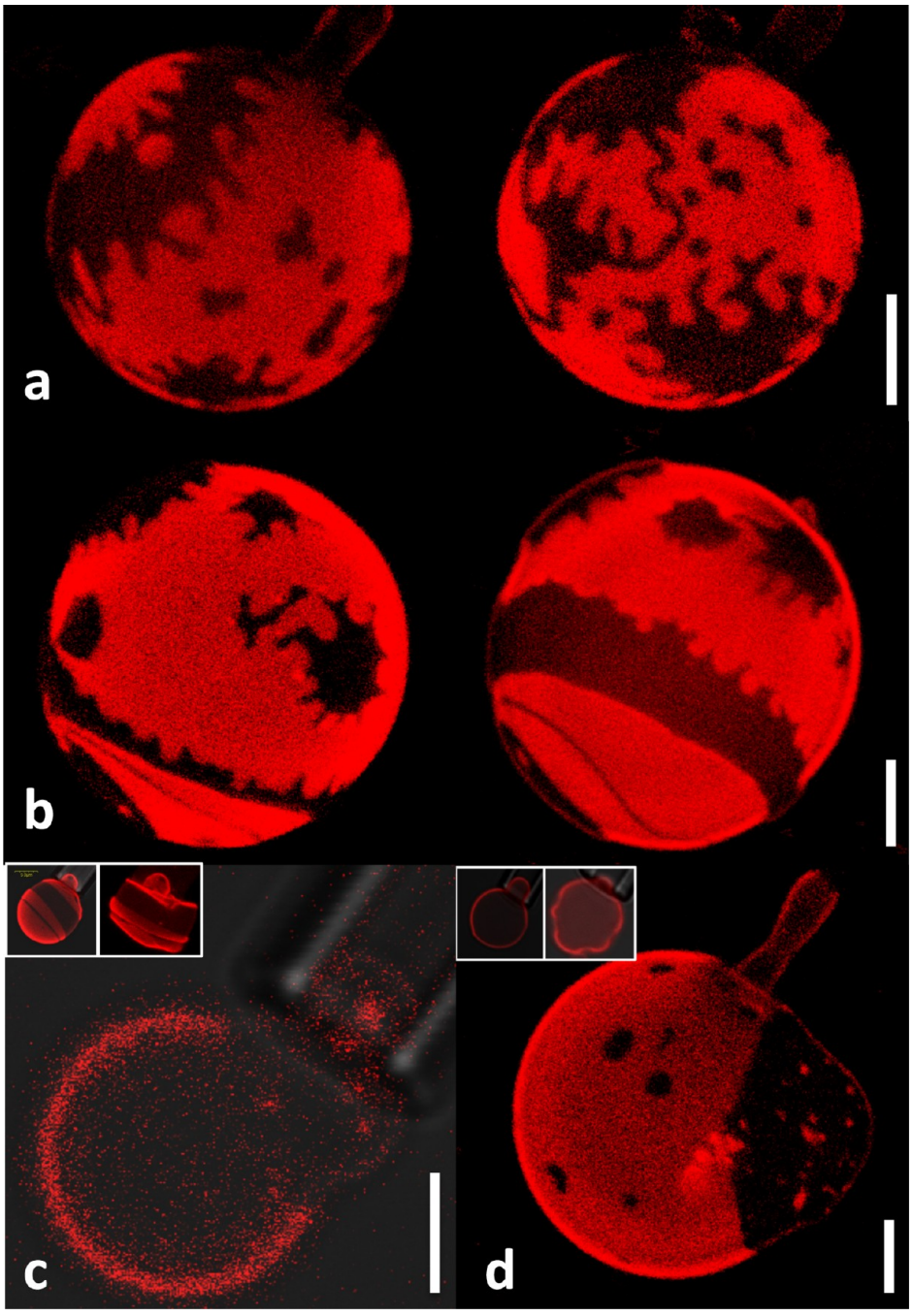

Figure 3. Domain morphologies in phase-separated vesicles with a weight ratio of AB1/OB18* = 50:50 after adding NaOH. Confocal *z*-stack hemispheres displaying fingering domains imaged (a) 24 and (b) 48 h after adding 0.6 mM NaOH to the vesicle dispersion. No systematic difference in domain patterns was observed with time. (c) Equatorial section of a dumbbell-shaped vesicle imaged 24 h after 0.6 mM NaOH addition. The AB1-rich phase is aspirated into the micropipet at 150 Pa, which suggests a softening of the AB1-rich phase. Insets in panel c are vesicles before NaOH treatment (left) and under osmotic deflation by evaporation (right). The creased, folded configurations reveal the original solid feature of AB1-rich domains. (d) AB1-rich domain positive curvature induced by the chain repulsion in the outer leaflet after 24 h of NaOH treatment. Insets in panel d are vesicles before NaOH treatment, from which we see either no curvature or negative curvature of AB1-rich domains. The scale bar is 5 μm.

interdiffusion of OB18* during domain demixing induced by EDTA stimuli, a simple diffusion model according to Fick's second law is applied

$$D\frac{1}{r}\frac{\partial}{\partial r}\left(r\frac{\partial C}{\partial r}\right) = \frac{\partial C}{\partial t} \quad (1)$$

where C is the concentration of OB18* in the mixing AB1-rich domain, r is the radius of the AB1-rich domain, and D is the interdiffusion coefficient of OB18*. Together with the continuity equation, an effective diffusion coefficient can be calculated (details in Appendix I):

$$D_E = \frac{1}{4\pi}\frac{A_0 - A}{t} \quad (2)$$

By fitting the above equation to the plot of the AB1-rich domain area versus time (Figure 2d), we calculated the effective

dx.doi.org/10.1021/la304602e | *Langmuir* XXXX, XXX, XXX−XXX

interdiffusion coefficient of OB18* to be $D_E = (2.3 \pm 0.5) \times 10^{-5}$ $\mu m^2/s$ ($N_{domain} = 17$, $N_{vesicle} = 4$).

The interdiffusion coefficient of OB18* is orders of magnitude smaller than OB18* self-diffusion (0.0024 $\mu m^2/s$).[34] This smaller diffusion coefficient could be due to the asymmetric application of EDTA to the outer leaflet only. Inner leaflets of AB1-rich domains are not in contact with EDTA, which limits the bilayer OB18* interdiffusion according to the domain registration. Further interpretation of the interdiffusion coefficient requires an experimental understanding of the domain registration mechanism, which is unclear even in lipid bilayer systems. However, recent coarse-grained molecular dynamics (CGMD) simulations suggest the raft registration arises spontaneously in bilayers with a calcium cross-linked ordered phase segregated from a liquid disordered phase.[25] Calcium straightens the cross-bridged chains, all the way into the hydrophobic core (Figure 1b). Any perturbation that interrupts the registration of rafts of straightened chains will also induce a thickness mismatch between phases and a "bump" in the opposing liquid-phase leaflet. This local curvature mismatch is sufficient to guide rafts together and stabilize the registered state. However, the EDTA effects confirm that calcium cross-bridging of negatively charged PAA chains plays an essential role in the phase separation of polymer vesicles.

3.2. Calcium Chelation Results in a Decrease in the Overall AB1 Area Fraction. Phase-separated vesicles composed of either 25 wt % AB1 (Figure 2e) or 60 wt % AB1 (Figure 2f) were used to characterize the kinetics of the overall AB1 area fraction effect following EDTA addition (either 0.48 or 0.83 mM). When fit with a single-exponential decay, the domain dynamics in 25 wt % vesicles are very weakly dependent on the EDTA concentration. Both concentrations of EDTA can be fit with a time constant of 19 min. The 60 wt % vesicles produce fits with time constants of 9 to 10 min for 0.48 and 0.83 mM EDTA, which again demonstrates a weak dependence on EDTA concentration. The results show that roughly doubling the weight percentage of AB1 roughly doubles the rate of domain shrinkage, and although 60 wt % vesicles show higher EDTA shrinkage domains more so than lower EDTA shrinkage domains, the rate results otherwise indicate a weak dependence on EDTA concentration. This suggests that remixing kinetics are not reaction-limited but rather diffusion-limited. CGMD simulations lend some molecular-scale insight: a phase-separated bilayer with a molecular cross-linker shows a stably registered domain (Figure 1b, upper image), followed by the removal of all of the cross-linkers from the upper leaflet, which produces a dissolution of the periphery of the upper domain with diffusive intermixing (Figure 1b, lower image). More experiments could lend deeper insight, but the present results certainly highlight the importance of Ca^{2+} for the maintenance of phase separation by polyanion cross-briding.

3.3. Increasing the pH by NaOH Incubation. In addition to calcium, another key factor controlling the phase behavior is the pH, which could modulate calcium condensation onto PAA chains in a critical concentration range.[23] To test the domain change upon losing H^+ from PAA chains in the outer leaflet of vesicle, we increased the pH by adding NaOH at concentrations ranging from 0.15 to 6.25 mM. To control for the addition of sodium ions by NaOH, NaCl was added to phase-separated vesicle suspensions at equal concentration with no observed alteration to the domain size or shape (data not shown). Therefore, phenomena observed upon addition of NaOH are most likely due to the increase in the charge on the PAA chains that results from the increase in pH as well as the osmotic pressure between chains resulting from Na^+ replacing free H^+.

Changes in the domain shape and area fraction were not obviously dependent on the NaOH concentration. However, the speed of vesicle disintegration accelerates as the NaOH concentration increases (data not shown). Near the upper bound of the NaOH concentration tested (6.25 mM), a resulting pH of 7.9 causes vesicles to break down into membrane patches or wormlike micelles within hours. Because the focus of this study is on changes in domain architecture rather than vesicle stability, NaOH treatments were limited to a regime where vesicles remained intact.

Upon addition of NaOH, the increasing pH leads to the deprotonation of carboxylic groups of the PAA chains, which become increasingly more negatively charged. The removal of H^+ causes metal ions from solution to bind to PAA chains. However, as our earlier investigation pointed out, the entropy penalty, favoring mixing, associated with confining counterions to PAA-rich domains increases with counterion concentration.[23] Calcium cannot be confined in PAA chains at high concentrations, and the electrostatic repulsion between PAA chains increases. Another possible mechanism for the observation of sprawling domains is that whereas NaOH removes H^+ ions, Na^+ ions are incorporated with the PAA brushes, which induces an osmotic pressure increase and "pushes" the brushes apart. Domain persistence under asymmetric NaOH treatment allowed the observation of dramatic changes in domain morphology such as viscous fingering, bulging AB1-rich domains, and a change in the domain area fraction.

3.3.1. Fingering in Mixing/Demixing and In-Plane Swelling of AB1-Rich Domains. The treatment of phase-separated polymersomes with NaOH for several hours is asymmetric with respect to leaflet perturbations and results in a small number (~10%, $N_{vesicle} = 30$) of vesicles exhibiting fingering domain boundaries (Figure 3a,b). This fingering pattern could be due to the swelling and softening of AB1-rich domains with increasing interchain electrostatic repulsion. As previously shown, AB1-rich domains are calcium cross-bridged gels that cannot be aspirated into a micropipet at low aspiration pressures (<200 Pa).[23] Furthermore, AB1-rich domains show irregular rigid creases under osmotic deflation (Figure 3c, insets), which also suggests gel-like AB1-rich domains. In contrast, incubation with NaOH softens AB1-rich domains to a liquidlike state as evidenced by facile aspiration into the micropipet (Figure 3c). The AB1-rich domain deformed while being projected into the pipet and later disassembled, resulting in the failure of vesicle integrity (data not shown). Therefore, liquid-like AB1-rich domains are not mechanically stable after NaOH stimulus because of the electrostatic repulsion between chains.

The addition of NaOH increases the electrostatic repulsion between AB1 chains, which maximizes the distance between AB1 chains and favors sprawling domains. Therefore, NaOH treatment leads to the growth of the AB1/OB18* domain interface length. A similar fingering pattern is found in phase-separated giant lipid vesicles close to a temperature-dependent mixing/demixing critical point.[5] It is likely that these NaOH-treated phase-separated polymersomes are approaching a mixing/demixing critical point because the rigidity difference between the AB1 and OB18* phases decreases with the softening of the AB1-rich domains. Although mixing/demixing is induced differently, chemically versus physically, phase-separated polymersomes and liposomes display a similar phenomenon as they reach a mixing/demixing critical point.

dx.doi.org/10.1021/la304602e | Langmuir XXXX, XXX, XXX–XXX

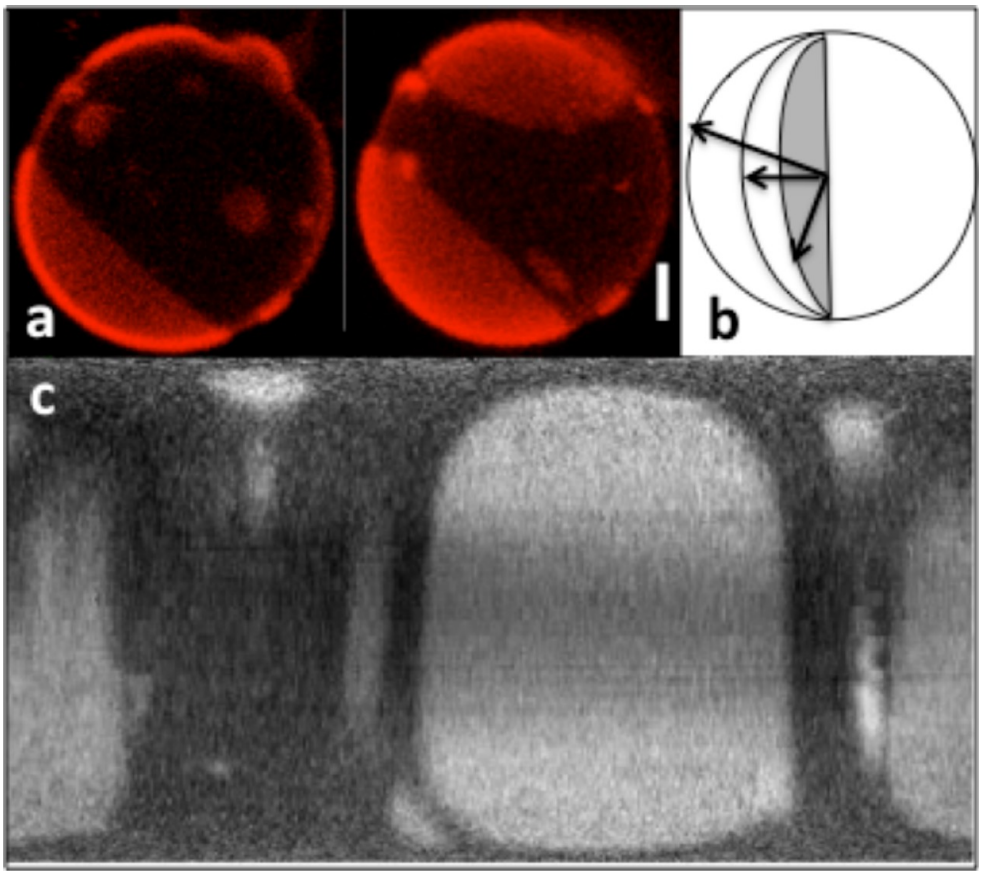

Figure 4. (a–c) Demonstration of the equal-area surface-mapping tool used for vesicle area fraction analysis. (a) Confocal *z*-stack hemispheres of a representative phase-separated vesicle with the mixing ratio AB1/OB18* = 50:50. The scale bar is 2 μm. (b) Schematic demonstration of the working principle of the mapping tool. The center point and the vesicle radius are estimated from the *z*-stack image of the vesicle and generate a sphere accordingly. The fluorescence intensities on the vesicle surface were obtained by searching along a line (indicated in red) perpendicular to the sphere surface for the maximum intensities. (c) 2D equal-area mapping of the phase-separated vesicle shown in panel a, for which the AB1-rich domain area fraction is calculated to be 0.518.

3.3.2. Bending Outward: Three-Dimensional AB1-Rich Domain Swelling. In addition to viscous fingering, nearly 14% ($N_{vesicle}$ = 30) of vesicles have AB1-rich domains bulging outward (Figure 3d) after incubation with NaOH. This positive curvature is in contrast to the AB1-rich domains in untreated vesicles that mostly display no curvature or negative curvature (Figure 3d, insets). We propose that the change in curvature of AB1-rich domains results from the difference in the interfacial area of AB1 molecules in the outer and inner leaflets. As NaOH is added to alter the pH asymmetrically, the repulsion between PAA chains in the outer leaflet leads to the expansion of the AB1 molecular area, whereas the AB1 molecular area remains constant in the inner leaflet. When the outer leaflet has more area compared to the inner leaflet, the domain bends outward. Therefore, the change in membrane curvature in AB1-rich domains reflects leaflet asymmetry after NaOH treatment.

3.3.3. Decreasing Area Fraction: Slow Partial Remixing of AB1/OB18.* After NaOH is added, the area fraction of AB1-rich domains decreases because of the mixing of AB1-rich and OB18*-rich domains. To estimate the extent of mixing, we quantify the area fraction of each phase per vesicle. A surface-mapping tool was developed that projects the 3D vesicle surface onto an equal-area 2D map. The working principle of the algorithm is obtained by searching for the maximum fluorescence intensity along lines normal to the surface of the sphere calculated from the estimation of the center and the radius of the vesicle. A confocal *z* projection of an example vesicle (Figure 4a) with a mixing ratio of AB1/OB18* = 50:50 w/w (51:49 mol/mol) is mapped to a 2D surface (Figure 4b,c), from which the AB1-rich domain area fraction was calculated to be 51.8%.

With this mapping tool, the domain area fractions were calculated at different mixing ratios. AB1-rich domain area fractions of vesicles were measured to be 22 ± 5% (av ± S.E., $N_{vesicle}$ = 5) and 48 ± 2% ($N_{vesicle}$ = 11) for AB1 weight fractions of 25 and 50%, respectively. However, after the NaOH stimulus, the AB1-rich domain area fractions were reduced after overnight incubation as shown in area fraction plots (Figure 5a). Average values of AB1-rich domain area fractions were significantly decreased to 10 ± 1% ($N_{vesicle}$ = 5, $p < 0.05$) for a 25% AB1 weight fraction and 33 ± 4% ($N_{vesicle}$ = 19, $p < 0.005$) for a 50% AB1 weight fraction. The decrease in the AB1 area fraction reveals the increase in miscibility of AB1 in OB18*-rich domains after NaOH treatment, which also impacts the domain shape (Figure 5b). The miscibility between AB1 and OB18* is tuned by the electrostatic repulsion between charged PAA chains, which is sensitive to changes in pH. As expected from previous work,[23] increasing the pH without changing the calcium concentration will result in the slow mixing of the phase-separated polymersome membrane when compared to the kinetics of EDTA treatment.

3.4. Removal of Both Calcium and H^+ by Adding EDTA Plus NaOH. In addition to adding EDTA and NaOH

dx.doi.org/10.1021/la304602e | *Langmuir* XXXX, XXX, XXX–XXX

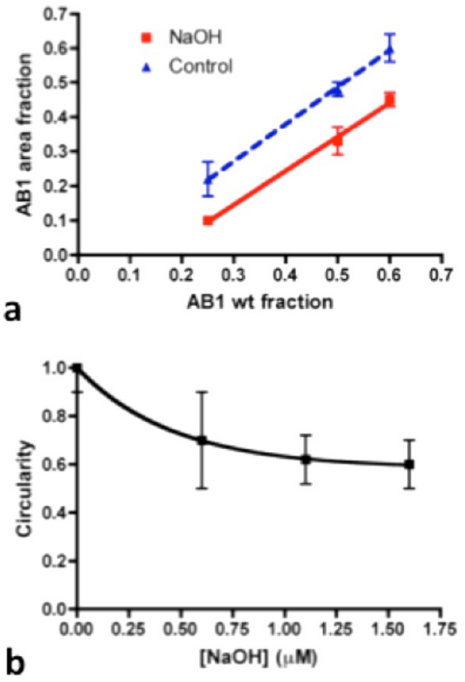

Figure 5. (a) AB1-rich domain area fraction plot as a function of AB1 weight fraction before (blue triangles) and after (red squares) NaOH treatment. The average AB1 area fractions are 60 ± 4% (av ± S.E., $N_{vesicle}$ = 5, before NaOH) and 45 ± 2% (avg ± S.E., $N_{vesicle}$ = 5, after NaOH) for an AB1 weight fraction of 60%, 48 ± 2% (av ± S.E., $N_{vesicle}$ = 11, before NaOH) and 33 ± 4% (av ± S.E., $N_{vesicle}$ = 19, after NaOH) for an AB1 weight fraction of 50%, and 22 ± 5% (av ± S.E., $N_{vesicle}$ = 5, before NaOH) and 10 ± 1% (av ± S.E., $N_{vesicle}$ = 5, after NaOH) for an AB1 weight fraction of 25%. Solid and dashed lines are linear fits to squares and triangles, respectively. The parallel trend of these two lines indicates that the changes in area fractions after NaOH treatment are roughly identical for different mixing ratios. Linear fits: before NaOH addition, $y = (0.98 \pm 0.06)x$, $R^2 = 1.0$; after NaOH addition, $y = (1.08 \pm 0.04)x$, $R^2 = 1.0$. (b) Effect of NaOH on individual domain circularity. After 24 h of incubation, domain circularity is reduced in a dose-dependent manner. Fit: $y = 0.42 \exp[-x/0.46] + 0.58$, N_{domain} = 8.

independently, a mixture of EDTA and NaOH in a molar ratio of 1:8 was added to 25 and 60% AB1 phase-separated polymersome dispersions. We found that a small amount of EDTA accelerated and enhanced the effects of NaOH on domain morphology. For example, almost all of the vesicles showed fast (in minutes) boundary roughening when adding both EDTA and NaOH, whereas only 10% of vesicles undergo slow (hours) boundary roughening while being incubated with NaOH alone. The EDTA added here, 0.09 mM, is much less concentrated compared to the previous EDTA-only application (0.36−0.96 mM). However, the calcium concentration reached a lower value under the former condition. The reason is that EDTA calcium chelation is more efficient at higher pH.

Domain morphology deviates from circular domains within minutes (Figure 6a). To measure the loss of the circular domain morphology quantitatively upon addition of EDTA and NaOH, the circularity of domains was calculated as circularity = 4π(area/perimeter^2) and plotted versus time (Figure 6b). The decrease in the domain circularity with time results from the electrostatic repulsion between AB1 molecules. The decreasing circularity is fitted with an exponential decay resulting in circularity = $e^{-t/\tau}$ (τ = 25 min, N_{domain} = 4). As the small decay constant indicates, a fast (within 10 min) boundary roughening process is achieved with the assistance of EDTA addition compared to slow (more than 4 h) domain kinetics induced by NaOH treatment alone. In addition to changes in circularity, changes in the vesicle surface area were observed as the swelling of the entire vesicle (Figure 6a). This increase in vesicle surface area is likely a result of increases in the AB1-rich domain area (indicated using arrows in Figure 6a) induced by the swelling of the PAA chains after the loss of calcium cross-bridging as well as increased interchain repulsion by deprotonation. As expected, the measurement of the AB1-rich domain area using the 2D mapping tool corresponded well to the total surface area increase of the vesicle in Figure 5a. Both showed an increase of about 130 μm^2. However, no systematic area fraction changes were obtained because of the fast vesicle disassembly upon adding both EDTA and NaOH. The addition of both NaOH and EDTA in an 8:1 ratio results in increased dynamics and loss of domain circularity.

4. DISCUSSION

As the schematic phase diagram in Figure 7 illustrates, external chemical stimuli were applied to phase-separated vesicles (white star), by which the system was shifted out of the region of phase separation (pink region) in roughly three directions: decreasing [H^+] (black line), decreasing [Ca^+] (blue line), and decreasing both [H^+] and [Ca^{2+}] (red line). Decreases in [Ca^{2+}] were achieved by the addition of excess concentrations of calcium-chelating agent EDTA. Once calcium was removed from the AB1-rich domains in the outer leaflet of the vesicle, domains began mixing within minutes. The addition of NaOH increased the pH and subsequently induced decreases in AB1-rich domain area fractions and fingering domain boundary patterns and changes in AB1-rich domain curvature. A commonality in both EDTA and NaOH effects is the mixing behavior of AB1-rich and OB18*-rich domains. In both cases, domain mixing results from a disruption of the calcium cross-bridging that induces the lateral segregation of AB1 into domains either by the removal of calcium by chelation or by increasing calcium entropy. The difference in mixing kinetics upon EDTA and NaOH stimuli could be due to these different mechanisms for cross-bridge disruption, where the decrease in the area of AB1-rich domains upon EDTA addition shows fast (minutes−hours) total mixing and the area fraction decrease induced by NaOH features slow (hours−days) partial mixing. The difference in mixing speed reflects the sensitivity of AB1-rich domains, changing from solid to fluid, upon external stimuli and is consistent with our previous finding that the effective rigidity of AB1 membranes is more sensitive to changes in calcium concentration than pH.[23] Although the mixing kinetics are faster with EDTA addition, large increases in pH have a more dramatic effect on the total vesicle architecture. As seen in the gray region of Figure 6, vesicles become unstable within minutes after being doused with high concentrations of NaOH as they disassemble to form worms or membrane patches. We propose that the strong electrostatic repulsion between PAA chains at such large increases in pH (pH 3.5−7.9) gives rise to leaky vesicles. Importantly, at physiological pH (pH 7.4) phase-separated polymersomes remain intact and undergo slow partial domain mixing. This stability presents promise for the application of spotted polymersomes in controlled drug release under physiological conditions.

Domain registration across the inner and outer leaflets of polymer bilayer membranes is suggested from the phenomenon under asymmetric chemical treatment. Domain registration became clear when mapping 3D z-stack projections to 2D area maps revealed no third, intermediate fluorescence intensity.

dx.doi.org/10.1021/la304602e | Langmuir XXXX, XXX, XXX−XXX

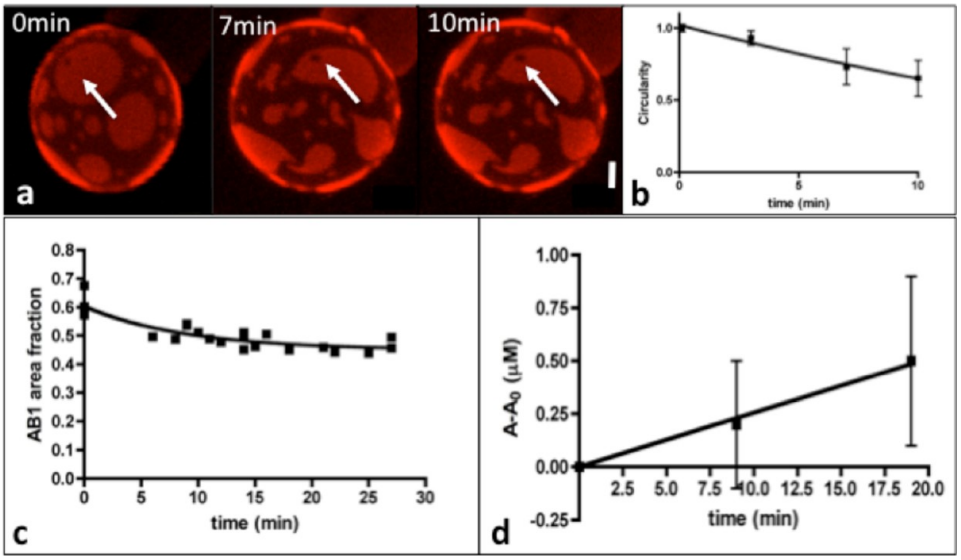

Figure 6. Domain roughening is observed within minutes upon combined EDTA and NaOH addition. (a) Time lapse images upon adding 0.09 mM EDTA and 0.72 mM NaOH. The domain morphology deviates from circular domains within minutes, which is much faster than the kinetics of NaOH treatment alone. The scale bar is 2 μm. (b) Circularities of AB1-rich domains decrease with time ($N_{domain} = 4$), which is calculated using circularity = 4π(area/perimeter^2). The black line is the exponential fit to the data, circularity = 1.38 exp$[-t/31.82] - 0.36$, for which the half-life is calculated to be 22 min. (c) Effect of overall AB1 area fraction after the addition of 1:8 EDTA/NaOH. Exponential fit: $y = 0.15 \exp[-t/8.95] + 0.45$, $R^2 = 0.81$, $N_{vesicle} = 6$. although EDTA addition alone shows AB1 domain shrinkage, the addition of EDTA and NaOH displays an enlargement of individual AB1 domains. Linear fit: $y = -(0.026 \pm 0.001)t$, $P < 0.002$, $N_{domain} = 4$.

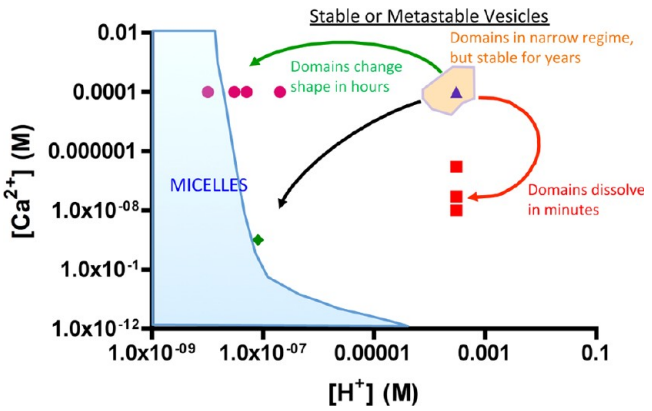

Figure 7. Phase diagram illustrating pH and $[Ca^{2+}]$ shifts. The orange area denotes the hydration solution conditions where the phase separation of polymer vesicles composed of AB1 and OB18* can be found.[23] The blue diamond is the hydration condition that we began with in this study, which is pH 3.5 and $[Ca^{2+}] = 0.1$ mM. Chemicals were added to vesicle dispersions reaching an external condition as denoted by the colored markers. The green line denotes the treatment with NaOH, leading to an increase in pH. Domain boundary roughening and area fraction decrease occur within hours to days. The black line represents the treatment with NaOH plus a small amount of EDTA (8:1 NaOH/EDTA). Boundary roughening occurs within minutes. The red line depicts EDTA treatment that chelates calcium from the outer leaflet of the vesicles, thus inducing fast domain mixing within minutes. The blue region of the phase diagram designates the limit of vesicle stability upon adding EDTA and/or NaOH. Calcium concentrations were calculated from the apparent formation constants of the EDTA–Ca^{2+} complex at different pH values.[28] The pH was measured using pH test strips.

Domain registration is generally accepted in lipid systems such as membrane "rafts," planar lipid bilayers, and giant unilamellar lipid vesicles (GUV). Although several hypotheses of trans bilayer coupling exist for lipid membranes, including cholesterol translocation, chain interdigitation, domain interfacial tension, and electrostatic potential across the membrane,[35] a definitive theory remains elusive. For polymer vesicles, polymer translocation is not possible because flip-flop is prevented by the high molecular weight of the polymer. However, we cannot exclude other mechanisms mentioned above. In addition to the above hypothesis, the possibility of domain registration suggested here is the domain curvature. The phenomenon of different curvatures shown in different types of domains confirms the domain registration hypothesis and suggests a curvature-induced interleaflet coupling mechanism that has just recently been confirmed by CGMD simulations that show chain ordering within domains due to the ligand cross-bridging of chains.[24] The experimental observations are consistent with results from Naumann and co-workers, who also suggest that the interleaflet coupling of polymer-tethered lipid bilayer coupling may aid the understanding of cell membrane leaflet coupling and offer new insights into this important topic.[36]

The work here extends such findings with kinetics and provides experimental observations of the roles that divalent ligands play in stabilizing phase separation within polymersomes. Furthermore, although the alteration of the surrounding chemical milieu is shown to disrupt phase separation, interleaflet registration is maintained. These finding may provide motivation for future applications in drug delivery platforms or contrast agents for in vivo tissue imaging.

APPENDIX

According to Fick's second law, diffusion-like behavior in cylindrical systems is shown in eq 1. Assuming that diffusion is slow enough for the system to reach steady state, eq 1 can be simplified to the following differential equation

$$\frac{\partial}{\partial r}\left(r\frac{\partial C}{\partial r}\right) = 0 \qquad \text{(A1)}$$

dx.doi.org/10.1021/la304602e | Langmuir XXXX, XXX, XXX–XXX

and boundary conditions

$$C|_{r=R_0} = C_0$$
$$C|_{r=R_m} = 0 \quad \text{(A2)}$$

where C_0 is the OB18* concentration in OB18* domain, as illustrated in Figure 2c. R_0 is the original AB1 domain radius at $t = 0$, and R_m is the moving radius of the AB1 domain by the invading OB18* phase. Solving eq A2, we obtain

$$\frac{C}{C_0} = \frac{\ln(r/R_m)}{\ln(R_0/R_m)} \quad \text{(A3)}$$

Given the continuity equation

$$-\frac{\partial R_m}{\partial t}C_0 = D\frac{\partial C}{\partial r}\bigg|_{R_m} \quad \text{(A4)}$$

$(\partial C)/(\partial r)|R_m = (C_o)/(R_m \ln(R_o/R_m))$ calculated from eq A3 is inserted into eq A4. We integrate eq A4 over the interval $[R_0, R_m]$. It follows that

$$\frac{1}{4}(1 - x^2) + \frac{1}{2}x^2 \ln x = \frac{Dt}{{R_0}^2} \quad \text{(A5)}$$

where $x = R_m/R_0 < 1$. Neglecting terms higher than second order in x, eq A5 is then simplified to

$$\frac{1}{4}({R_0}^2 - {R_m}^2) = Dt \quad \text{(A6)}$$

from which the diffusion coefficient formula shown in eq 2 is obtained.

AUTHOR INFORMATION

Corresponding Author

*E-mail: baumgart@sas.upenn.edu, discher@seas.upenn.edu.

Author Contributions

K.S. and A.T. contributed equally to this work.

Notes

The authors declare no competing financial interest.

ACKNOWLEDGMENTS

This work was supported by the UPenn MRSEC grant from the National Science Foundation (award no. DMR05-20020) and by NIH EB007049 (D.E.D.).

REFERENCES

(1) Juliano, R. L. Liposomes as a drug deliver system. *Trends Pharmacol. Sci.* **1981**, *2*, 39−42.

(2) Christian, D. A.; Cai, S.; Bowen, D. M.; Kim, Y.; Pajerowski, J. D.; Discher, D. E. Polymersome carriers: from self-assembly to siRNA and protein therapeutics. *Biopharmaceutics* **2009**, *71*, 463−474.

(3) de Almeida, R. F. M.; Borst, J. W.; Fedorov, A.; Prieto, M.; Visser, A. J.W.G. Complexity of lipid domains and rafts in giant unilamellar vesicles revealed by combining imagine and microscopic and macroscopic time-resolved fluorescence. *Biophys. J.* **2007**, *93*, 539−553.

(4) Baumgart, T.; Hess, S. T.; Webb, W. W. Imaging coexisting fluid domains in biomenbrane models coupling curvature and line tension. *Nature* **2003**, *425*, 821−824.

(5) Veatch, S. L.; Keller, S. L. Separation of liquid phases in giant vesicles of ternary mixtures of phospholipids and cholesterol. *Biophys. J.* **2003**, *80*, 3074−3083.

(6) Dietrich, C.; Bagatolli, L. A.; Volovyk, Z. N.; Thompson, N. L.; Levi, M.; Jacobson, K.; Gratton, E. Lipid rafts reconstituted in model membranes. *Biophys. J.* **2000**, *80*, 1417−1428.

(7) Bagatolli, L. A.; Gratton, E. Two photon fluorescence microscopy of coexisting lipid domains in giant unilamellar vesicles of binary phospholipid mixtures. *Biophys. J.* **2000**, *78*, 290−305.

(8) Yanagisawa, M.; Imai, M.; Taniguchi, T. Shape deformation of ternary vesicles coupled with phase separation. *Phys. Rev. Lett.* **2008**, *100*, 148102.

(9) Heinrich, M.; Tian, A.; Esposito, C.; Baumgart, T. Dynamic sorting of lipids and proteins in membrane tubes with a moving phase boundary. *Proc. Natl. Acad. Sci. U.S.A.* **2010**, *107*, 7208−7213.

(10) Haverstick, D. M.; Glaser, M. Visualization of Ca^{2+}-induced phospholipid domains. *Proc. Natl. Acad. Sci. U.S.A* **1987**, *84*, 4475−4479.

(11) Shoemaker, S. D.; Vanderlick, T. K. Calcium modulates the mechanical properties of anionic phospholipid membranes. *J. Colloid Interface Sci.* **2003**, *266*, 314−321.

(12) Discher, B. M.; Won, Y. Y.; Ege, D. S.; Lee, J. C-M.; Bates, F. S.; Discher, D. E.; Hammer, D. A. Polymersomes: tough vesicles made from diblock copolymers. *Science* **1999**, *284*, 1143−1146.

(13) Discher, D. E.; Eisenberg, A. Polymer vesicles. *Science* **2002**, *297*, 967−972.

(14) Discher, D. E.; Ahmed, F. Polymersomes. *Annu. Rev. Biomed. Eng.* **2006**, *8*, 323−341.

(15) Fernyhough, C.; Ryan, A. J.; Battaglia, G. pH controlled assembly of a polybutadiene-poly(methacrylic acid) copolymer in water: packing considerations and kinetic limitations. *Soft Matter* **2009**, *5*, 1674−1682.

(16) Konradi, R.; Ruhe, J. Interaction of poly(methacrylic acid) brushes with metal ions: an infrared investigation. *Macromolecules* **2004**, *37*, 6954−6961.

(17) Currie, E. P. K.; Sieval, B.; Fleer, G. J.; Cohen Stuart, M. A. Polyacrylic acid brushes: surface pressure and salt-induced swelling. *Langmuir* **2000**, *16*, 8324−8333.

(18) Konradi, R.; Ruhe, J. Interaction of poly(methacrylic acid) brushes with metal ions: swelling properties. *Macromolecules* **2005**, *38*, 4345−4354.

(19) Shen, L.; Du, J.; Armes, S. P.; Liu, S. Kinetics of pH-induced formation and dissociation of polymeric vesicles assembled from a water-soluble zwitterionic diblock copolymer. *Langmuir* **2008**, *24*, 10019−10025.

(20) Lee, A. S.; Butun, V.; Vamvakaki, M.; Armes, M. P.; Pople, J. A.; Gast, A. P. Structure of pH-dependent block copolymer micelles: charge and ionic strength dependence. *Macromolecules* **2002**, *35*, 8540−8551.

(21) Geng, Y.; Ahmed, F.; Bhasin, N.; Discher, D. E. Visualizing worm micelle dynamics and phase transitions of a charged diblock copolymer in Water. *J. Phys. Chem. B* **2005**, *109*, 3772−3779.

(22) Cui, H.; Chen, Z.; Zhong, S.; Wooley, K. L.; Pochan, D. J. Block copolymer assembly via kinetic control. *Science* **2007**, *317*, 647−650.

(23) Christian, D. A.; Tian, A.; Ellenbroek, W. G.; Levental, I.; Rajagopal, K.; Janmey, P. A.; Liu, A. J.; Baumgart, T.; Discher, D. E. Spotted vesicles, striped micelles and Janus assemblies induced by ligand binding. *Nat. Mater.* **2009**, *8*, 843−849.

(24) Pantano, D. A.; Moore, P. B.; Klein, M. L.; Discher, D. E. Raft registration across bilayers in a molecularly detailed model. *Soft Matter* **2011**, *7*, 8182−8191.

(25) Tian, A.; Baumgart, T. Sorting of lipids and proteins in membrane curvature gradients. *Biophys. J.* **2009**, *96*, 2676−2688.

(26) Opsteen, J. A.; Cornelissen, J. J. L. M.; van Hest, J. C. M. Block copolymer vesicles. *Pure Appl. Chem.* **2004**, *76*, 1309−1319.

(27) Battaglia, G.; Ryan, A. J.; Tomas, S. Polymeric vesicle permeability: a facile chemical assay. *Langmuir* **2006**, *22*, 4910−4913.

(28) Horkay, F.; Tasaki, I.; Basser, P. J. Osmotic swelling of polyacrylate hydrogels in physiological salt solutions. *Biomacromolecules* **2000**, *1*, 84−90.

(29) Martell, A. E.; Smith, R. M. *Critical Stability Constants*; Plenum Press: New York, 1974; Vol. *1*, pp 204−211.

(30) Samsonov, A. V.; Mihalyov, I.; Cohen, F. S. Characterization of cholesterol-sphingomyelin domains and their dynamics in bilayer membranes. *Biophys. J.* **2001**, *81*, 1486−1500.

(31) Garg, S.; Ruhe, J.; Ludtke, K.; Jordan, R.; Naumann, C. A. Domain registration in raft-mimicking lipid mixtures studied using polymer-tethered lipid bilayers. *Biophys. J.* **2007**, *92*, 1263−1270.

(32) Bermudez, H.; Hammer, D. A.; Discher, D. E. Effect of bilayer thickness on membrane bending rigidity. *Langmuir* **2004**, *20*, 540−543.
(33) Dlubek, G.; Bondarenko, V.; Pionteck, J.; Kilburn, D.; Pompe, G.; Taesler, C.; Redmann, F.; Petters, K.; Krause-Rehberg, R.; Alam, M. A. Studies of interdiffusion in polymer blends by PALS. *Radiat. Phys. Chem.* **2003**, *68*, 369−373.
(34) Lee, J.C.-M.; Santore, M.; Bates, F. S.; Discher, D. E. From membranes to melts, rouse to reptation: diffusion in polymersome versus lipid bilayers. *Macromolecules* **2002**, *35*, 323−326.
(35) Collins, M. D. Interleaflet coupling mechanisms in bilayers of lipid and cholesterol. *Biophys. J.* **2008**, *94*, L32−L34.
(36) Deverall, M. A.; Garg, S.; Ludtke, K.; Jordan, R.; Ruhe, J.; Naumann, C. A. Transbilayer coupling of obstructed lipid diffusion in polymer-tethered phospholipid bilayers. *Soft Matter* **2008**, *4*, 1899−1908.